LETTER • OPEN ACCESS

Entropy production of active Brownian particles going from liquid to hexatic and solid phases

A Letters Journal Exploring the Frontiers of Physics

November 2024

EPL, **148** (2024) 37001
doi: 10.1209/0295-5075/ad895e

www.epljournal.org

Entropy production of active Brownian particles going from liquid to hexatic and solid phases

Massimiliano Semeraro[1(a)], Giuseppe Negro[2], Antonio Suma[1], Federico Corberi[3] and Giuseppe Gonnella[1]

[1] *Dipartimento Interateneo di Fisica, Università degli Studi di Bari and INFN, Sezione di Bari via Amendola 173, Bari I-70126, Italy*
[2] *School of Physics and Astronomy, University of Edinburgh - Peter Guthrie Tait Road, Edinburgh, EH9 3FD, UK*
[3] *Dipartimento di Fisica "E. R. Caianiello", Università degli Studi di Salerno and INFN, Gruppo Collegato di Salerno - via Giovanni Paolo II 132, I-84084 Fisciano (SA), Italy*

received 2 September 2024; accepted in final form 21 October 2024
published online 13 November 2024

Abstract – Due to its inherent intertwinement with irreversibility, entropy production is a prime observable to monitor in systems of active particles. In this numerical study, entropy production in the liquid, hexatic and solid phases of a two-dimensional system of active Brownian particles is examined at both average and fluctuation level. The trends of averages as functions of density show no singularity and marked changes in their derivatives at the hexatic-solid transition. Distributions show instead peculiar tail structures interpreted by looking at microscopic configurations. Particles in regions of low local order generate tail values according to different dynamical mechanisms: they move towards empty regions or bounce back and forth into close neighbours. The tail structures are reproduced by a simple single-particle model including an intermittent harmonic potential.

Introduction. – In statistical mechanics, *entropy production* quantifies irreversibility of thermodynamical processes due to breaking of time-reversal symmetry: a positive value is a distinctive hallmark of non-equilibrium states and provides a measurement of their degree of irreversibility [1–6]. Furthermore, entropy production also proved to be a valuable tool for characterizing non-equilibrium phase transitions [7,8]. As shown by numerous studies about master equations [9,10], chemical [11,12], Ising-like [13–15], lattice [14,16,17], field [18] and active matter models [8,19–26], close to transition points or at the boundary between phase-separated states entropy production (or its derivative) peaks or even diverges. One can thus naturally wonder how general this behaviour is.

Investigation of average values but also of *fluctuations* of entropy production and related thermodynamical observables is central to fully characterize non-equilibrium systems. In this respect, *large deviations theory* [27,28] already had a deep impact in non-equilibrium statistical mechanics [29–35]. A key concept here is the *large deviation principle*. For a quantity $\mathcal{S}_\tau$ integrated over a time τ, this is satisfied if the asymptotics of its probability distribution $p(\mathcal{S}_\tau/\tau = s)$ can be described in terms of the *rate function* $I(s) \equiv \lim_{\tau\uparrow\infty} \ln(p(\mathcal{S}_\tau/\tau = s))/\tau$. Large deviations theory outperforms the central limit theorem as $I(s)$ assigns fluctuations of any amplitude an occurrence probability, and is additionally identified as a non-equilibrium analogue of free energy.

The study of large deviations already proved successful in detecting peculiar fluctuation regimes. For a single Brownian particle, the rate function for the work injected by the thermal bath features a strictly convex central regime together with left and right linear stretches connected through second-order singular points [36,37]. Similar results were found for single active particles and active work, *i.e.*, particles driven by a self-propulsion force and work performed by the latter [38]. In both cases, linear stretches were associated to rare trajectories with

(a) E-mail: massimiliano.semeraro@uniba.it (corresponding author)

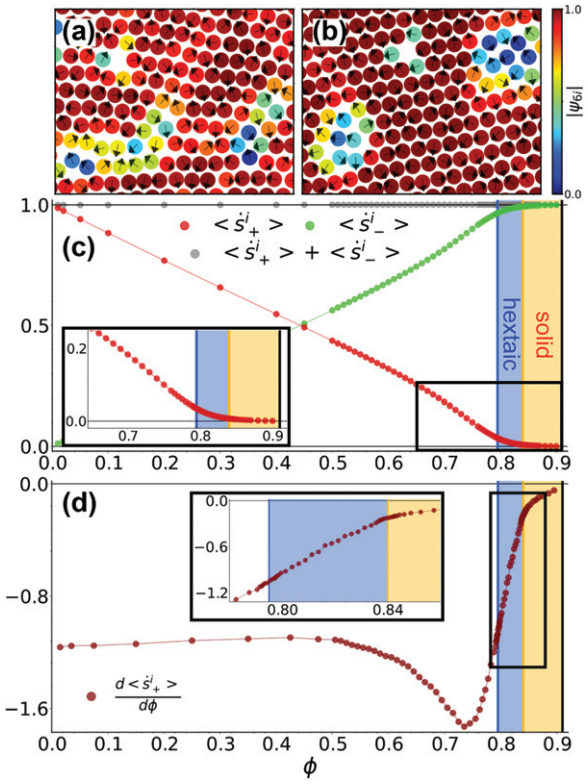

Fig. 1: (a) and (b): snapshots of a portion of the system at $\phi = 0.82$ in the hexatic phase and $\phi = 0.85$ in the solid one, respectively. Particles are coloured according to their $|\psi_{6i}|$. (c) $\langle \dot{s}^i_\pm \rangle$ and $\langle \dot{s}^i_+ \rangle + \langle \dot{s}^i_- \rangle$ as functions of ϕ. The horizontal black lines report the limiting values $0, 1$, the blue and yellow rectangles in the background highlight the regions of hexatic and solid order, with the two coloured vertical lines denoting the transition densities $\phi_{lh} \simeq 0.795$ and $\phi_{hs} \simeq 0.84$ [45] and the black one denoting the close packing $\phi_{cp} \simeq 0.91$. The inset reports an enlargement of the area enclosed into the rectangle. (d) $\mathrm{d}\langle \dot{s}^i_+ \rangle / \mathrm{d}\phi$ as a function of ϕ with an enlargement of the area enclosed into the rectangle. In all panels $Pe = 10$ and $N = 256^2$ are fixed.

large initial/final values, or *big jumps*. Singular behaviours for active work were also discovered in large systems of active particles [39]. Here linear stretches were traced back to particles dragged by small clusters against their self-propelling direction.

In this letter, we focus on Active Brownian Particles (ABPs) [40–44] in two dimensions and study how phase transitions at high density are reflected by the behaviour of entropy production at both average and fluctuation level. We also relate entropy production to the dynamics of topological defects characterizing these transitions. The phase diagram of ABPs has been carefully described in [45]. Here we consider intermediate activities for which at high enough densities a liquid-hexatic and an hexatic-solid phase transitions occur, with the hexatic and solid phases characterized by quasi–long-range orientational and translational order, respectively (see fig. 1(a) and (b)). We find that the average entropy production as a function of density is not affected by any discontinuity, thus it cannot be employed as an order parameter. However, its derivative marks the hexatic-solid transition density with a pronounced change. Concerning fluctuations, in the liquid phase the log-probabilities result strictly convex, while in the ordered phases at intermediate times they show linear stretches or two-minima structures. We explain these features by looking at the trajectories of particles generating different entropy production contributions. Typically, particles locally arranged in hexatically ordered configurations are essentially locked and contribute to the convex part around the global minimum, while particles in regions of low local order or in proximity to vacancies result more mobile and contribute to the other branches. Finally, we propose a single-particle model able to reproduce these peculiar features by incorporating key dynamical aspects of the original one through an intermittent harmonic potential.

Model. – We consider N ABPs moving in a periodic square box of side L. Each ABP has unit diameter σ_d, self-propels due to a force $\boldsymbol{a}_i = F_a \hat{\boldsymbol{n}}_i$ with constant amplitude F_a and direction $\hat{\boldsymbol{n}}_i = (\cos\theta_i, \sin\theta_i)$ and has its dynamics ruled by the following Langevin equations:

$$m\ddot{\mathbf{r}}_i = -\gamma\dot{\mathbf{r}}_i + F_a\hat{\boldsymbol{n}}_i - \sum_{i\neq j} \nabla U_i(r_{ij}) + \sqrt{2\gamma k_B T}\,\boldsymbol{\xi}_i,$$
$$\dot{\theta}_i = \sqrt{2D_\theta}\,\eta_i, \qquad (1)$$

where i, j label particles, m is their mass, $\boldsymbol{r}_i$ is the position of the i-th particle, γ is the friction coefficient, k_B is the Boltzmann constant, T is the environment temperature and $\boldsymbol{\xi}_i$ and $\boldsymbol{\eta}_i$ are two independent zero-mean white noises which satisfy $\langle \boldsymbol{\xi}_i(t)\boldsymbol{\xi}_j(s)\rangle = \delta_{ij}\delta(t-s)\mathbf{1}$ and $\langle \eta_i(t)\eta_j(s)\rangle = \delta_{ij}\delta(t-s)$. Particles interact via the shifted and truncated Mie potential $U(r) = 4\epsilon[(\sigma_d/r)^{64} - (\sigma_d/r)^{32}] + \epsilon$ if $r < r_c = 2^{1/32}\sigma_d$ and 0 otherwise, with ϵ energy unit and r_c location of the potential minimum. D_θ is a positive constant which is related to the self-propulsion persistence time as $\tau_p = 1/D_\theta$, whence the persistence length $l_P = \tau_p F_a/\gamma$. As in [46,47], we choose the convention $D_\theta = 3k_BT/(\sigma_d^2\gamma)$ which relates translational and rotational diffusion of spherical particle (see the Supplementary Material `Supplementarymaterial.pdf` (SM) for details). We consider three different system sizes, $N = 128^2, 256^2$ and 512^2, so as to address possible finite size effects. Moreover, in order to explore the ABP phase diagram from [45], we introduce the density $\phi = N\pi\sigma_d^2/(4L^2)$, with ϕ_{lh}, ϕ_{hs} and $\phi_{cp} \simeq 0.91$ denoting the liquid-hexatic and hexatic-solid transition densities and the close packing fraction, respectively, and the Péclet number $Pe = F_a\sigma_d/(k_BT)$, which compares the strength of the self-propulsion to thermal fluctuations. In the following we fix $m = 1$, $\gamma = 10$, $k_BT = 0.05$ and $\epsilon = 1$ so that the system is consistent with the overdamped picture and $\tau_p \simeq 66.67$. σ_d, m and ϵ serve as our length, mass and energy units [48]. For each system size, we

explore the phase diagram region $10 \leq Pe \leq 30$ without MIPS [45]. To monitor positional and orientational order, we introduce particle-wise the number of nearest neighbours n_i, which is extracted from a Voronoi tessellation, and the local hexatic order parameter ψ_{6i}, which is defined as $\psi_{6i} = \psi_6(\boldsymbol{r}_i) \equiv \sum_{j=1}^{n_i} e^{\imath 6\theta_{ij}}/n_i$. Here n_i denotes the number of neighbours of the i-th particle, while θ_{ij} is the angle formed between the segment connecting the centres of the i-th particle and its j-th neighbour and the x-axis. Details about numerical integration and sampling are reported in the SM.

Entropy production. – In active particles systems, entropy production is an important subject [49–54] as parity of active force under time reversal transformation is not uniquely determined [8,55–60]. In principle, one could arbitrarily consider the active force either odd or even, as both choices are equally possible and supported by physical interpretations [57,59–61]. Accordingly, two different expressions for the entropy production rate emerge,

$$\dot{\tilde{\mathcal{S}}}^i_+ \equiv \lim_{\tau\uparrow\infty} \frac{1}{\tau}\frac{F_a}{k_BT}\int_0^\tau \hat{\boldsymbol{n}}_i(s)\dot{\mathbf{r}}_i(s)\,\mathrm{d}s = \lim_{\tau\uparrow\infty}\dot{\tilde{s}}^i_+, \quad (2)$$

$$\dot{\tilde{\mathcal{S}}}^i_- \equiv \lim_{\tau\uparrow\infty} \frac{1}{\tau}\frac{F_a}{\gamma k_BT}\sum_{i\neq j}\int_0^\tau \hat{\boldsymbol{n}}_i(s)\nabla_i U(r_{ij})\,\mathrm{d}s = \lim_{\tau\uparrow\infty}\dot{\tilde{s}}^i_-, \quad (3)$$

where the subscripts $\pm$ denote the active force is assumed even or odd (see the SM for details on vanishing boundary terms). Interestingly, these two expressions are not disconnected. One can in fact prove that $\langle\dot{\tilde{\mathcal{S}}}^i_+\rangle + \langle\dot{\tilde{\mathcal{S}}}^i_-\rangle = \langle\dot{\tilde{s}}^i_+\rangle + \langle\dot{\tilde{s}}^i_-\rangle = F_a^2/(\gamma k_BT) \equiv c_s$ particle-wise (see the SM for derivation). In the following we thus normalize the rates as $\dot{s}^i_\pm \equiv \dot{\tilde{s}}^i_\pm/c_s$ so that they become adimensional with range in $[0,1]$. We remark that $\dot{\tilde{\mathcal{S}}}^i_+$ is strictly related to the rate of active work, from which it differs only for a $1/T$ factor [39,50,53,57,62–64]. We underline that active work is a fundamental observable in active systems as it captures the energy cost to sustain self-propulsion [50,53,57,63], its distribution can be singular [38,39,64] and it defines the efficiency for active engines [53,65].

Average trends. – Firstly, note that $\dot{\mathcal{S}}^i_\pm$ sense particle aggregation. $\dot{\mathcal{S}}^i_+$ is large and positive when $\hat{\boldsymbol{n}}_i(s)\dot{\mathbf{r}}_i(s) > 0$, *i.e.*, when particles are driven by their activity unhindered by other particles, while it is large and negative when $\hat{\boldsymbol{n}}_i(s)\dot{\mathbf{r}}_i(s) < 0$, *i.e.*, when particles are dragged against their activity. $\dot{\mathcal{S}}^i_-$ is instead large and positive when $\hat{\boldsymbol{n}}_i(s)\nabla_i U(r_{ij}) > 0$, *i.e.*, when particles are in close contact and push each other driven by activity.

To make these remarks more quantitative, we look first at averages at $Pe = 10$ and $N = 256^2$. In fig. 1(c) we report the trends of $\langle\dot{s}^i_\pm\rangle$ as functions of ϕ sampled over $\tau = 10^3 \gg \tau_p$. Let us focus on $\langle\dot{s}^i_+\rangle$ first. Note that, as ϕ is increased from 0 to $\phi_{cp} \simeq 0.91$, particles have their mobility increasingly reduced and $\langle\dot{s}^i_+\rangle$ decreases from 1 to 0. In particular, $\langle\dot{s}^i_+\rangle$ decreases linearly up to $\phi \simeq 0.5$, *i.e.*, well inside the dilute liquid phase. Notably, at larger ϕ $\langle\dot{s}^i_+\rangle$ seems to sense phase transitions. In fact, as shown by the inset in fig. 1(c), as soon as particles start to order first orientationally at $\phi_{lh} \simeq 0.795$ and then positionally at $\phi_{hs} \simeq 0.84$ [45], the decrease rate reduces until asymptotically zeroing at ϕ_{cp}. This point is corroborated by the derivative reported in fig. 1(d). It is in fact almost constant up to $\phi = 0.5$. At $\phi \sim 0.75$ it is interested by a bump which we attribute to the increased aggregation effect of activity at such densities. Reflecting the inset of fig. 1(c), at larger densities the derivative is instead strictly increasing, and also shows a marked change around ϕ_{hs} which mirrors the passage from the hexatic phase, in which particles are still mobile, to the solid one, in which, apart from defects, they arrange orderly according to an hexagonal pattern (see fig. 1(a) and (b)). We remark that our results are in agreement with [54,66], where total entropy production rate for active solids is shown to reduce as ϕ is increased.

Figure 1(c) shows that symmetric comments apply to $\langle\dot{s}^i_-\rangle$. In figs. S1 and S2 from the SM we confirm this scenario to hold for different N and a larger Pe. We conclude remarking that, as shown in fig. 1(c), the sum rule $\langle\dot{s}^i_+\rangle + \langle\dot{s}^i_-\rangle = 1$ is satisfied at every ϕ. We thus focus on $\dot{s}^i_+$.

Fluctuations. – We now turn to the investigation of fluctuations, instrumental to better clarify the relation between entropy production and microscopic evolution. We sample $\dot{s}^i_+$ from all particles over increasing τ so as to estimate the curves $-\ln(p(\dot{s}^i_+))/\tau$, with $p(\dot{s}^i_+)$ probability distribution at corresponding τ. In fig. 2(a)–(d) we report such curves at $\phi = 0.1$ in a very dilute configuration and at $\phi = 0.76$, 0.82, 0.85 well inside the liquid, hexatic and solid phases, respectively. In each case τ spans from $\tau = 5 \cdot 10 \simeq \tau_p$ to $\tau = 10^3 \gg \tau_p$. Looking first at fig. 2(a), we observe that the right branches of the curves collapse perfectly on each other, while the left branches do not, but rather tend to slightly flatten towards the horizontal axis. This is reminiscent of what found in [39], where at similar packing fractions but much larger Pe the distribution of the active work rate is characterized by collapsing right branches and flattening left linear branches. In [39], this peculiar behaviour is ascribed to particles behaving in two different ways during sampling: some move freely without ever impacting other particles and then contributing to the right branches essentially as independent free particles, whereby collapse of the curves is expected; the remainder that contribute to the left branches are instead often dragged against their active forces by small clusters, hence increasing the probability of negative $\dot{s}^i_+$ values. Apart from particles bouncing into each other instead of being dragged due to our lower Pe, in our case the overall phenomenology is essentially the same. We therefore move to our novel results at larger ϕ. Figure 2(b) relative to $\phi = 0.76$ shows that both branches of $-\ln(p(\dot{s}^i_+))/\tau$ have

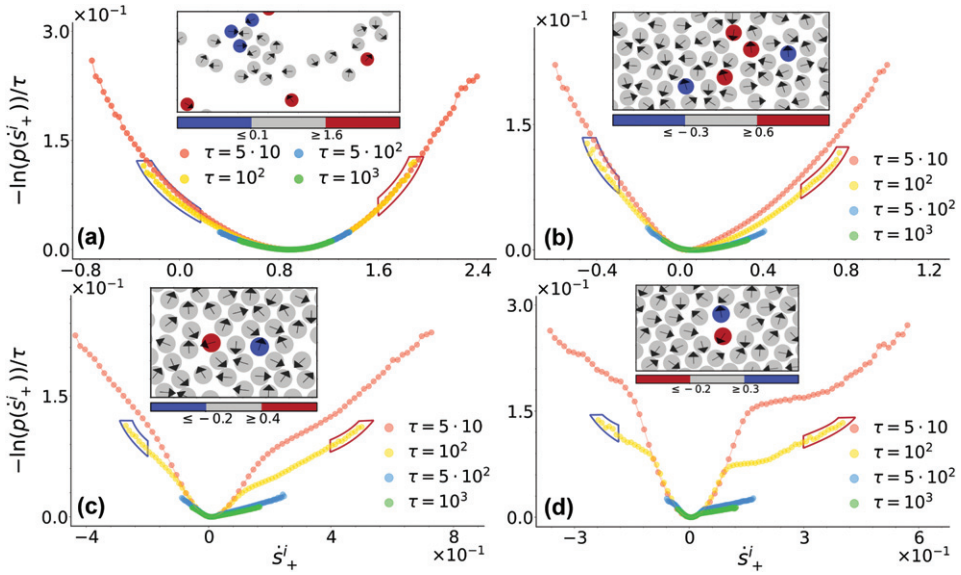

Fig. 2: (a)–(d) Curves $-\ln(p(\dot{s}^i_+))/\tau$ at $\phi = 0.1$, 0.76, 0.82 and 0.85, respectively. For comparison, here and in the following these curves are shifted in such a way that their minimum is null. In each panel curves are coloured according to the τ during which $\dot{s}^i_+$ were sampled. Insets report snapshots of a portion of the system at corresponding ϕ. As denoted by the horizontal bars, particles are coloured in red, grey and blue according to their $\dot{s}^i_+$ values sampled over $\tau = 10^2 \simeq \tau_p$. The left and right conditional intervals are highlighted in the main panels by boxes with matching colours. Black arrows denote the instantaneous direction of the activity at the final sampling instant.

reduced convexity and tend to flatten. As for fig. 2(c) and (d) relative to $\phi = 0.82, 0.85$, we instead observe a net distinction between a central parabolic regime around $\dot{s}^i_+ \simeq \langle \dot{s}^i_+ \rangle \simeq 0$ and left and right branches with peculiar shapes, the latter attaching to the parabolic region at decreasing $\dot{s}^i_+$ as τ is increased. An intuition about these peculiar shapes is provided by the insets of fig. 2, which report snapshots with particles coloured according to their $\dot{s}^i_+$ values sampled over $\tau = 10^2 \simeq 1.5\tau_p$ (yellow points in the main panels). As apparent from the inset of fig. 2(d), we observe that $\dot{s}^i_+$ values close to $\langle \dot{s}^i_+ \rangle$ and far in the tails seem to be associated to particles trapped in regions of high local positional order and with more freedom of movement in regions of low local one.

In order to quantitatively support this intuition, we now relate $\dot{s}^i_+$ to $|\psi_{6i}|$, n_i values. In fig. 3(a)–(c) we report snapshots of the system at $\phi = 0.82$ with particles respectively coloured according to their $\dot{s}^i_+$, $|\psi_{6i}|$ and n_i values (see figs. S3 and S5 in the SM for similar figures at $\phi = 0.76$ and 0.85). To better access $\dot{s}^i_+$ values far in the tails, here we reduce the sampling interval to $\tau = 10 < \tau_p$. ψ_{6i}, n_i are instead extracted at the final sampling instant. Interestingly, a quick comparison between panels reveals that particles with $\dot{s}^i_+ \sim \langle \dot{s}^i_+ \rangle$ are often characterized by final $|\psi_{6i}| \sim 1$, $n_i = 6$ values, while particles with $|\dot{s}^i_+| \gg \langle \dot{S}^i_+ \rangle$ are associated to $\psi_{6i} < 1$, $n_i < 6$ values. Hence the former are hexatically ordered, while the latter are located close or even into vacancies at the final time. Complementary information is provided by the sample trajectories from fig. 3(d)–(f) associated to particles from the upper panels highlighted by matching rectangles: fig. 3(d) shows that large positive values are due to particles moving towards regions where free space is available, so that velocity and activity are often parallel; the irregular trajectory from fig. 3(e) remarks instead that negative values are associated to particles still moving in freer regions, but often bouncing into or pushed by close neighbours, so that now velocity and activity are often anti-parallel; finally fig. 3(f) shows that values close to average are due to particles which remain essentially locked due to the trapping exerted by close neighbours. A more direct visualization of the mechanisms just described is offered by the supplementary movies `Video_S1_phi_0.76.mp4`, `Video_S2_phi_0.82.mp4` and `Video_S3_phi_0.85.mp4`. The consistency of this scenario during the entire time interval is instead proved in fig. 3(g). Here we report the distribution of $|\bar{\psi}_{6i}|$, *i.e.*, of the modulus of ψ_{6i} time-averaged over τ, conditioned on the intervals $\dot{s}^i_+ \gg \langle \dot{s}^i_+ \rangle$, $\dot{s}^i_+ \ll \langle \dot{s}^i_+ \rangle$ and $\dot{s}^i_+ \simeq \langle \dot{s}^i_+ \rangle$ highlighted in the inset. It is apparent that for particles with $\dot{s}^i_+ \simeq \langle \dot{s}^i_+ \rangle$, $|\bar{\psi}_{6i}| \sim 1$, *i.e.*, these particles remain essentially locally hexatically ordered over the entire sampling interval. On the contrary, particles associated to high and low $\dot{s}^i_+$ values are characterized by $|\bar{\psi}_{6i}| < 1$ values, *i.e.*, they are located in regions of low local hexatic order. Figure S6 from the SM shows that an analysis of $\bar{n}_i$ leads to coherent and complementary results.

A phenomenological model. – Having grasped the essential dynamical aspects generating peculiar distribution shapes, we now introduce a simple single-particle model incorporating the former and reproducing the latter. The basic idea is the following: when in regions of

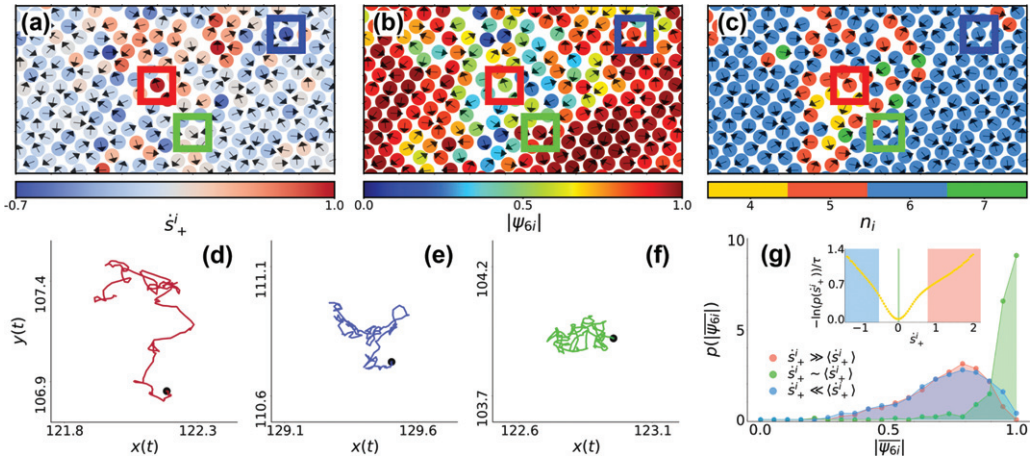

Fig. 3: (a)–(c) Snapshots of a portion of the system at $\phi = 0.82$. Particles are coloured according to their $\dot{s}^i_+$, $|\psi_{6i}|$ and n_i values, the former sampled over $\tau = 10$, the latter two extracted at the final sampling instant. Rectangles are instrumental to the bottom panels. (d)–(f) Sample trajectories relative to the centre of particles with $\dot{s}^i_+ \simeq 1.04, -0.76$ and $8.74 \cdot 10^{-3}$, the first two far in the tails, the latter $\sim \langle\dot{s}^i_+\rangle \sim 1.22 \cdot 10^{-2}$ (see inset of (g)). Black dots denote the trajectories initial points, while their colours matches the rectangle from (a)–(c) individuating the particles they belong to. For comparison, in all panels the x and y axes span the same interval length $0.7\sigma_d$. (g) Distributions of $|\bar{\psi}_{6i}|$ conditioned on $\dot{s}^i_+ \simeq \langle\dot{s}^i_+\rangle \sim 1.22 \cdot 10^{-2}$, $\dot{s}^i_+ \geq 0.8 \gg \langle\dot{s}^i_+\rangle$ and $\dot{s}^i_+ \leq -0.5 \ll \langle\dot{s}^i_+\rangle$. The inset reports the curve $-\ln(p(\dot{s}^i_+))/\tau$ for $\tau = 10$ built using $\dot{s}^i_+$ values from all particles. Rectangles in the background are coloured according to the legend from the main panels and highlight the conditioning intervals.

high (low) local order, particles are considered effectively trapped (free). The simple phenomenological model we therefore employ is inspired by Brownian resetting studies and includes a single ABP under the action of an intermittent harmonic potential [67–69]:

$$\begin{aligned} m\ddot{\boldsymbol{r}} &= -\gamma\dot{\mathbf{r}} + F_a\hat{\boldsymbol{n}} - k\lambda(t)\boldsymbol{r}(t) + \sqrt{2\gamma k_B T}\,\boldsymbol{\xi}, \\ \dot{\theta} &= \sqrt{2D_\theta}\,\eta. \end{aligned} \tag{4}$$

Here k is the elastic constant of a harmonic potential $U(\boldsymbol{r}) = k\boldsymbol{r}^2/2$ and $\lambda(t)$ is a dichotomous noise alternatively taking values 0 and 1, while all other symbols keep the same meaning as in eq. (1). The time intervals $\tilde{\tau}$ during which $\lambda(t)$ is 0 or 1 are extracted from the exponential distributions $p_{f/h}(\tilde{\tau}) = e^{-\tilde{\tau}/\tau_{f/h}}/\tau_{f/h}$, $\tilde{\tau} \geq 0$, where the subscript f (h) refers to $\lambda(t) = 0$ (1). The average fraction of times during which the particle is free or confined thus are $\zeta_{f/h} = \tau_{f/h}/(\tau_f + \tau_h)$. We fix $\tau_f = \tau_p$ and set $\tau_h = \alpha \cdot \tau_f$, $\alpha > 0$. The first equality ensures that the ABP is on average free for intervals τ_p during which at $Pe \sim 10$ it travels distances $l_p \sim 3 \sim \sigma_d$ comparable to the ones usually travelled by particles in regions of low local order (see fig. 1(a) and (b)). The second one instead simply tunes τ_h with τ_f as reference: with $\alpha \gg 1$ ($\ll 1$) the particle is mostly trapped (free) like particles in regions of high (low) local order. We remark that once $\tau_h/\tau_f = \alpha$ is fixed, choosing a different τ_f only results in a rescaling of the times at which the same log-curves are observed.

We now provide proof that our simple model actually works. To reproduce results from the hexatic phase, in which particles are often far and softly impact each other, we set $Pe = 10, k = 1$ and $\alpha = 0.1$, so that $\zeta_h \sim 9\%$.

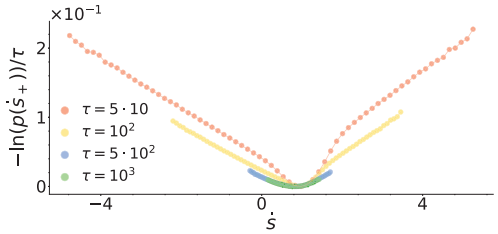

Fig. 4: Curves $-\ln(p(\dot{s}_+))/\tau$ at $Pe = 10$, $k = 1$, $\alpha = 0.1$ for different sampling times τ in the single-particle model equation (4).

The resulting curves $-\ln(p(\dot{s}_+)/\tau$ for our single ABP from fig. 4 clearly resemble the ones from fig. 2(c), with $\dot{s}_+$ values far in the tails and $\sim \langle\dot{s}_+\rangle$ due to particles trapped on average 50% $\gg \zeta_h$ and %5 $\sim \zeta_h$ of the time, respectively. As shown in fig. S7 from the SM, curves similar to the ones from fig. 2(b) and (d) relative to the liquid and solid phases can be obtained by fine tuning α. In general, as shown by the trajectories in fig. S7 in the SM high-$\dot{s}_+$ particles persistently move pushed by the active force while free, so that velocity and active force are often parallel. Instead, low-$\dot{s}_+$ particles are often trapped when far away from the centre of the potential, so that while being pushed towards it their velocities and active forces are often anti-parallel. These mechanisms thus reproduce the motion of particles in regions of low local order which either move towards empty space or bounce into neighbours.

Conclusions. – In this letter, we numerically studied entropy production rates for large systems of ABPs both at the average and fluctuation level. We explored regions

of the phase diagram in which MIPS does not occur, but rather the system transitions from a liquid to a hexatic and a solid phase upon increasing density. Concerning averages, we found their trends as functions of density to monotonically vary according to the degree of mobility of particles and closeness to neighbours without discontinuity, thus denying them the role of order parameters. Their derivatives mark instead a pronounced change around the hexatic-solid transition. Concerning fluctuations, at intermediate times we detected peculiar tail structures in distributions which we explained by looking at microscopic configurations. We found that values far in the tails are associated to particles in regions of low local order where they can either move towards empty regions or bounce into other particles. We proved the connection between tail values and lost local order by measuring particle-wise the local hexatic order parameter and neighbour number. We also introduced a simple single-particle model able to reproduce these peculiar distribution shapes. This is based on the idea that when in regions of high (low) local order, particles are effectively trapped (free), and therefore includes an intermittent harmonic potential. In the future we plan to perturb our system with an asymmetric ratchets potential [70–72] to study its effect on entropy fluctuations and thermodynamical efficiency of the resulting device. It would also be interesting to extend our analysis to dynamical transitions occurring in active matter models described through orientational order parameters [73].

* * *

Access to Bari ReCaS e-Infrastructure funded through PON Research and Competitiveness 2007–2013 Call 254 Action and to high-performance computing resources granted by the CINECA award No. ISCRA IsCb1 AcT made this work possible. MS, GN, AS, GG acknowledge financial support by MUR projects PRIN 2020/PFCXPE, PRIN 2022/HNW5YL, PRIN 2022 PNRR/P20222B5P9 and Quantum Sensing and Modelling for One-Health (QuaSiModO). FC acknowledges financial support by MUR PRIN 2022 PNRR.

Data availability statement: All data that support the findings of this study are included within the article (and any supplementary files).

REFERENCES

[1] Maes C. and Netočný K., *J. Stat. Phys.*, **110** (2003) 269.
[2] Andrieux D., Gaspard P., Ciliberto S., Garnier N., Joubaud S. and Petrosyan A., *Phys. Rev. Lett.*, **98** (2007) 150601.
[3] Andrae B., Cremer J., Reichenbach T. and Frey E., *Phys. Rev. Lett.*, **104** (2010) 218102.
[4] Seifert U., *Rep. Prog. Phys.*, **75** (2012) 126001.
[5] Landi G. T., Tomé T. and de Oliveira M. J., *J. Phys. A*, **46** (2013) 395001.
[6] Peliti L. and Pigolotti S., *Stochastic Thermodynamics: An Introduction* (Princeton) 2021.
[7] Shim P.-S., Chun H.-M. and Noh J. D., *Phys. Rev. E*, **93** (2016) 012113.
[8] Crosato E., Prokopenko M. and Spinney R. E., *Phys. Rev. E*, **100** (2019) 042613.
[9] Noa C. E. F., Harunari P. E., de Oliveira M. J. and Fiore C. E., *Phys. Rev. E*, **100** (2019) 012104.
[10] da Silva R., de Oliveira M. J., Tomé T. and Drugowich de Felício J. R., *Phys. Rev. E*, **101** (2020) 012130.
[11] Nguyen B., Seifert U. and Barato A. C., *J. Chem. Phys.*, **149** (2018) 045101.
[12] Seara D. S., Machta B. B. and Murrell M. P., *Nat. Commun.*, **12** (2021) 392.
[13] Zhang Y. and Barato A. C., *J. Stat. Mech.*, **2016** (2016) 113207.
[14] Barbosa O. A. and Tomé T., *J. Stat. Mech*, **2018** (2018) 063202.
[15] Martynec T., Klapp S. H. L. and Loos S. A. M., *New J. Phys.*, **22** (2020) 093069.
[16] Tomé T. and de Oliveira M. J., *Phys. Rev. Lett.*, **108** (2012) 020601.
[17] Barato A. C. and Hinrichsen H., *J. Phys. A*, **45** (2012) 115005.
[18] Suchanek T., Kroy K. and Loos S. A. M., *Phys. Rev. Lett.*, **131** (2023) 258302.
[19] Nardini C., Fodor E., Tjhung E., van Wijland F., Tailleur J. and Cates M. E., *Phys. Rev. X*, **7** (2017) 021007.
[20] Negro G., Carenza L. N., Lamura A., Tiribocchi A. and Gonnella G., *Soft Matter*, **15** (2019) 8251.
[21] Crosato E., Spinney R. E., Nigmatullin R., Lizier J. T. and Prokopenko M., *Phys. Rev. E*, **97** (2018) 012120.
[22] Caballero F. and Cates M. E., *Phys. Rev. Lett.*, **124** (2020) 240604.
[23] Favuzzi I., Carenza L. N., Corberi F., Gonnella G., Lamura A. and Negro G., *Soft Mater.*, **19** (2021) 334.
[24] Ferretti F., Grosse-Holz S., Holmes C., Shivers J. L., Giardina I., Mora T. and Walczak A. M., *Phys. Rev. E*, **106** (2022) 034608.
[25] Ro S., Guo B., Shih A., Phan T. V., Austin R. H., Levine D., Chaikin P. M. and Martiniani S., *Phys. Rev. Lett.*, **129** (2022) 220601.
[26] Paoluzzi M., Levis D., Crisanti A. and Pagonabarraga I., arXiv:2310.03423 (2024).
[27] Dembo A. and Zeitouni O., *Large Deviations Techniques and Applications*, 2nd edition (Springer, New York) 1988.
[28] den Hollander F., *Large Deviations* (AMS) 2000.
[29] Oono Y., *Prog. Theor. Phys. Suppl.*, **99** (1989) 165.
[30] Ellis R. S., *Entropy, Large Deviations, and Statistical Mechanics* (Springer) 2007.
[31] Lanford O. E., *Entropy and Equilibrium States in Classical Statistical Mechanics*, in *Statistical Mechanics and Mathematical Problems*, *Lect. Notes Phys.*, Vol. **20** (Springer) 2007, pp. 1–113.
[32] Touchette H., *Phys. Rep.*, **478** (2009) 1.
[33] Cecconi F., Cencini M., Puglisi A., Vergni D. and Vulpiani A., *From the Law of Large Numbers to Large*

Deviation Theory in Statistical Physics: An Introduction (Springer) 2014.
[34] Zamparo M. and Semeraro M., *J. Math. Phys.*, **64** (2023) 023302.
[35] Semeraro M., Suma A. and Negro G., *Entropy*, **26** (2024) 439.
[36] Farago J., *J. Stat. Phys.*, **107** (2002) 781.
[37] Carollo G. B., Semeraro M., Gonnella G. and Zamparo M., *J. Phys. A*, **56** (2023) 435003.
[38] Semeraro M., Gonnella G., Suma A. and Zamparo M., *Phys. Rev. Lett.*, **131** (2023) 158302.
[39] Cagnetta F., Corberi F., Gonnella G. and Suma A., *Phys. Rev. Lett.*, **119** (2017) 158002.
[40] Fily Y. and Marchetti M. C., *Phys. Rev. Lett.*, **108** (2012) 235702.
[41] Romanczuk P., Bär M., Ebeling W., Lindner B. and Schimansky-Geier L., *Eur. Phys. J. ST*, **202** (2012) 1.
[42] Bialké J., Löwen H. and Speck T., *EPL*, **103** (2013) 30008.
[43] Redner G. S., Hagan M. F. and Baskaran A., *Phys. Rev. Lett.*, **110** (2013) 055701.
[44] Negro G., Caporusso C. B., Digregorio P., Gonnella G., Lamura A. and Suma A., *Eur. Phys. J. E*, **45** (2022) 75.
[45] Digregorio P., Levis D., Suma A., Cugliandolo L. F., Gonnella G. and Pagonabarraga I., *Phys. Rev. Lett.*, **121** (2018) 098003.
[46] Das S., Gompper G. and Winkler R. G., *New J. Phys.*, **20** (2018) 015001.
[47] Semeraro M., Suma A., Petrelli I., Cagnetta F. and Gonnella G., *J. Stat. Mech.*, **2021** (2021) 123202.
[48] Allen M. P. and Tildesley D. J., *Computer Simulation of Liquids* (Oxford University Press) 2017.
[49] Fodor E., Nardini C., Cates M. E., Tailleur J., Visco P. and van Wijland F., *Phys. Rev. Lett.*, **117** (2016) 038103.
[50] Mandal D., Klymko K. and DeWeese M. R., *Phys. Rev. Lett.*, **119** (2017) 258001.
[51] Pietzonka P. and Seifert U., *J. Phys. A*, **51** (2017) 01LT01.
[52] GrandPre T., Klymko K., Mandadapu K. K. and Limmer D. T., *Phys. Rev. E*, **103** (2021) 012613.
[53] Pietzonka P., Fodor E., Lohrmann C., Cates M. E. and Seifert U., *Phys. Rev. X*, **9** (2019) 041032.
[54] Caprini L., Marini Bettolo Marconi U., Puglisi A. and Löwen H., *J. Chem. Phys.*, **159** (2023) 041102.
[55] Puglisi A. and Marini Bettolo Marconi U., *Entropy*, **19** (2017) 356.
[56] Shankar S. and Marchetti M. C., *Phys. Rev. E*, **98** (2018) 020604.
[57] Dabelow L., Bo S. and Eichhorn R., *Phys. Rev. X*, **9** (2019) 021009.
[58] Caprini L., Marini Bettolo Marconi U., Puglisi A. and Vulpiani A., *J. Stat. Mech.*, **2019** (2019) 053203.
[59] Fodor E., Jack R. L. and Cates M. E., *Annu. Rev. Condens. Matter Phys.*, **13** (2022) 215.
[60] O'Byrne J., Kafri Y., Tailleur J. and van Wijland F., *Nat. Rev. Phys.*, **4** (2022) 167183.
[61] Oh Y. and Baek Y., *Phys. Rev. E*, **108** (2023) 024602.
[62] Nemoto T., Fodor É., Cates M. E., Jack R. L. and Tailleur J., *Phys. Rev. E*, **99** (2019) 022605.
[63] Ekeh T., Cates M. E. and Fodor E., *Phys. Rev. E*, **102** (2020) 010101.
[64] Keta Y.-E., Fodor É., van Wijland F., Cates M. E. and Jack R. L., *Phys. Rev. E*, **103** (2021) 022603.
[65] Fodor E. and Cates M. E., *EPL*, **134** (2021) 10003.
[66] Caprini L., Löwen H. and Marconi U. M. B., *J. Phys. A*, **56** (2023) 465001.
[67] Besga B., Bovon A., Petrosyan A., Majumdar S. N. and Ciliberto S., *Phys. Rev. Res.*, **2** (2020) 032029.
[68] Santra I., Das S. and Nath S. K., *J. Phys. A*, **54** (2021) 334001.
[69] Mercado-Vásquez G., Boyer D. and Majumdar S. N., *J. Stat. Mech.*, **2022** (2022) 093202.
[70] McDermott D., Reichhardt C. J. O. and Reichhardt C., *Soft Matter*, **12** (2016) 8606.
[71] Derivaux J.-F., Jack R. L. and Cates M. E., *J. Stat. Mech.*, **2022** (2022) 043203.
[72] Semeraro M., Gonnella G., Lippiello E. and Sarracino A., *Symmetry*, **15** (2023) 200.
[73] Head L. C., Doré C., Keogh R. R., Bonn L., Negro G., Marenduzzo D., Doostmohammadi A., Thijssen K., López-León T. and Shendruk T. N., *Nat. Phys.*, **20** (2024) 492.